NASA Technical Memorandum 106076

Thermoviscoplastic Analysis of Fibrous Periodic Composites Using Triangular Subvolumes

Kevin P. Walker
Engineering Science Software, Inc.
Smithfield, Rhode Island

Alan D. Freed
Lewis Research Center
Cleveland, Ohio

and

Eric H. Jordan
University of Connecticut
Storrs, Connecticut

March 1993

NASA

Thermoviscoplastic Analysis of Fibrous Periodic Composites Using Triangular Subvolumes

Kevin P. Walker
Engineering Science Software, Inc.
Smithfield, Rhode Island 02917

Alan D. Freed
NASA Lewis Research Center
Cleveland, Ohio 44135

Eric H. Jordan
University of Connecticut
Storrs, Connecticut 06268

Abstract

The nonlinear viscoplastic behavior of fibrous periodic composites is analyzed by discretizing the unit cell into triangular subvolumes. A set of these subvolumes can be configured by the analyst to construct a representation for the unit cell of a periodic composite. In each step of the loading history the total strain increment at any point is governed by an integral equation which applies to the entire composite. A Fourier series approximation allows the incremental stresses and strains to be determined within a unit cell of the periodic lattice. The nonlinearity arising from the viscoplastic behavior of the constituent materials comprising the composite is treated as a fictitious body force in the governing integral equation. Specific numerical examples showing the stress distributions in the unit cell of a fibrous tungsten/copper metal matrix composite under viscoplastic loading conditions are given. The stress distribution resulting in the unit cell when the composite material is subjected to an overall transverse stress loading history perpendicular to the fibers is found to be highly heterogeneous, and typical homogenization techniques based on treating the stress and strain distributions within the constituent phases as homogeneous result in large errors under inelastic loading conditions.

1 Introduction

Structural analysis of component hardware fabricated from composite materials requires the material to be considered as homogeneous. Methods for developing homogenized constitutive models for the composite rely on volume averaging the local stress-strain response in a small representative volume element of the composite material. Most methods approximate the local stress and

strain fields in the representative volume element as being homogeneous in each phase. If higher accuracy is required finite element representations of the local response can be obtained, but such finite element analyses would have to be carried out at each integration point in the global finite element analysis of the component at each step of the loading history. Such an approach leads to prohibitively long computation times.

In order to increase the accuracy of the local stress and strain field representations, and the efficiency in obtaining them, methods have been developed which can be embedded in the finite element calculations at each integration point. In previous papers[1,2] we developed a procedure for analyzing the nonlinear deformation behavior of periodic composites by means of Fourier's series and Green's functions. These methods are built upon work carried out in references 4–9 and 10–18, respectively. Both of these complementary approaches involve the solution of an integral equation for the total strain increment, in which the nonlinearity arising from viscoplasticity is treated as a fictitious body force. The loading history imposed on the composite is divided into discrete load steps, and the integral equation for the displacement increment in each load step is derived from Navier's equation when subject to incremental viscoplastic body forces. In the references cited[1,2], both approaches were shown to be equivalent to one another, and the Green's function formulation can be derived from the Fourier series representation by means of a Poisson sum technique. In another paper[3] the Fourier series approach was used to analyze the elastic behavior of a tungsten fiber/copper matrix (W/Cu) composite which is being considered as a substitute liner material to increase the strength and improve the durability of the combustion chambers in cryogenically-fuelled liquid propellant rocket engines. This analysis was carried out by discretizing the unit cell into rectangular subvolumes. In this paper we introduce a triangular discretization of the unit cell and perform a nonlinear viscoplastic analysis of periodic (W/Cu) composites. The rectangular and triangular subvolumes are the first two element geometries of a library of geometries, similar to a library of finite element geometries, that a user might wish to employ when performing a composite analysis.

In the following sections we develop numerical techniques which can be used to analyze the local stress and strain fields within the unit cell of a periodic composite. In an actual finite element calculation the unit cell would be discretized into a small number of subvolumes, and the local strain field values would be homogenized to provide the finite element code with the overall homogenized constitutive response at each integration point in the structure. Post-processing of the finite element results can then be carried out using a much finer discretization of the unit cell with the proposed numerical techniques.

2 Constitutive Equations

2.1 Hooke's Law

The form of Hooke's law suitable for infinitesimal strains can be written in the incremental form

$$\Delta\sigma_{ij}(\mathbf{r}) = D_{ijkl}(\mathbf{r})\left(\Delta\varepsilon^{\mathrm{T}}_{kl}(\mathbf{r}) - \Delta c_{kl}(\mathbf{r})\right), \tag{1}$$

in which $\Delta c_{kl}(\mathbf{r})$ is the strain increment representing the deviation from isothermal elastic behavior, i.e.

$$\Delta c_{kl}(\mathbf{r}) = \Delta\varepsilon^{\mathrm{P}}_{kl}(\mathbf{r}) + \alpha_{kl}(\mathbf{r})\,\Delta T(\mathbf{r}), \tag{2}$$

where at the point in the unit cell with position vector $\mathbf{r}$, $D_{ijkl}(\mathbf{r})$ is the elasticity tensor, $\Delta\varepsilon^{\mathrm{P}}_{kl}(\mathbf{r})$ is the inelastic strain increment, and $\alpha_{kl}(\mathbf{r})\,\Delta T(\mathbf{r})$ is the thermal strain increment. The inelastic strain increment can be computed explicitly at the point $\mathbf{r}$ since the stress is assumed to be known as a function of position $\mathbf{r}$ at the beginning of the increment. The only unknown quantity in equation (1) is then the total strain increment, $\Delta\varepsilon^{\mathrm{T}}_{kl}(\mathbf{r})$.

2.2 Evaluation of Total Strain Increment

The elasticity tensor at any point $\mathbf{r}$ in the composite material may be written in the form

$$D_{ijkl}(\mathbf{r}) = D^{\mathrm{m}}_{ijkl} + \delta D_{ijkl}(\mathbf{r}), \tag{3}$$

where

$$\delta D_{ijkl}(\mathbf{r}) = \vartheta(\mathbf{r})\left(D^{\mathrm{f}}_{ijkl} - D^{\mathrm{m}}_{ijkl}\right). \tag{4}$$

In this relationship $\vartheta(\mathbf{r}) = 1$ in the fiber and $\vartheta(\mathbf{r}) = 0$ in the matrix, with D^{f}_{ijkl} denoting the elasticity tensor of the fiber and D^{m}_{ijkl} that of the matrix. We then find[1-3] that in the Fourier series approach the total strain increment in the unit cell of a three dimensional periodic lattice is determined by solving the integral equation,

$$\begin{aligned}\Delta\varepsilon^{\mathrm{T}}_{kl}(\mathbf{r}) \;=\; & \Delta\varepsilon^{0}_{kl} + \frac{1}{V_c}\sum\sum_{n_p=0}^{\pm\infty}{\sum}' g_{klmn}(\boldsymbol{\zeta}) \times \\ & \times \iiint_{V_c} e^{i\boldsymbol{\xi}\cdot(\mathbf{r}-\mathbf{r}')}\left\{D^{\mathrm{m}}_{mnrs}\Delta c_{rs}(\mathbf{r}') - \delta D_{mnrs}(\mathbf{r}')\left[\Delta\varepsilon^{\mathrm{T}}_{rs}(\mathbf{r}') - \Delta c_{rs}(\mathbf{r}')\right]\right\} dV(\mathbf{r}'),\end{aligned} \tag{5}$$

where the fourth rank tensor $g_{klmn}(\boldsymbol{\zeta})$ is given by

$$g_{klmn}(\boldsymbol{\zeta}) = \frac{1}{2}\left(\zeta_n\zeta_l M^{-1}_{mk}(\boldsymbol{\zeta}) + \zeta_n\zeta_k M^{-1}_{ml}(\boldsymbol{\zeta})\right), \tag{6}$$

in which the Christoffel stiffness tensor $M_{ij}(\boldsymbol{\zeta})$, with inverse $M_{ij}^{-1}(\boldsymbol{\zeta})$, is defined[11,12] by the relation

$$M_{ij}(\boldsymbol{\zeta}) = D^{\mathrm{m}}_{pijq}\zeta_p\zeta_q, \tag{7}$$

with $\zeta_p = \xi_p/\sqrt{\xi_m\xi_m} = \xi_p/\xi$ being a unit vector in the direction of the Fourier wave vector $\boldsymbol{\xi}$, and $\xi = \sqrt{\xi_m\xi_m}$ denoting the magnitude of the vector $\boldsymbol{\xi}$. In equation (5) the sum is taken over integer values in which

$$\xi_1 = \frac{2\pi n_1}{L_1}, \quad \xi_2 = \frac{2\pi n_2}{L_2}, \quad \xi_3 = \frac{2\pi n_3}{L_3} \tag{8}$$

and L_1, L_2, L_3 are the dimensions of the unit periodic cell in the x_1, x_2, x_3 directions, so that the volume of the unit cell is given by the relation, $V_c = L_1L_2L_3$. The values of n_1, n_2, n_3 are given by

$$n_p = 0, \pm1, \pm2, \pm3, \ldots, \text{etc.}, \quad \text{for } p = 1,2,3 \tag{9}$$

and the prime on the triple summation signs indicates that the term with $n_1 = n_2 = n_3 = 0$ is excluded from the sum.

2.3 Evaluation of Viscoplastic Strain Increment

In solving the preceding integral equation for the total strain increment, $\Delta\varepsilon^{\mathrm{T}}_{kl}(\mathbf{r})$, it is first necessary to determine the inelastic strain increment, $\Delta\varepsilon^{\mathrm{P}}_{kl}(\mathbf{r})$, and thence the deviation strain increment, $\Delta c_{kl}(\mathbf{r})$, in equation (2).

For this purpose we use a simple viscoplastic constitutive relationship whose governing equations at a temperature of T° K are given in the form[19]:

$$\dot{\varepsilon}^{\mathrm{P}}_{ij} = \tfrac{1}{2}\|\dot{\boldsymbol{\varepsilon}}^{\mathrm{P}}\|\frac{S_{ij}}{\|S\|}, \tag{10}$$

$$\|\dot{\boldsymbol{\varepsilon}}^{\mathrm{P}}\| = \sqrt{2\dot{\varepsilon}^{\mathrm{P}}_{ij}\dot{\varepsilon}^{\mathrm{P}}_{ij}} = \theta(T)\,A\left(\frac{\|S\|}{C}\right)^n, \tag{11}$$

$$\theta(T) = \left\{\begin{array}{ll} \exp\left[-\dfrac{Q}{RT}\right] & \text{for} \quad T_t \le T < T_m \\ \exp\left[-\dfrac{Q}{RT}\left\{\ln\left(\dfrac{T_t}{T}\right)+1\right\}\right] & \text{for} \quad 0 \le T \le T_t \end{array}\right\}, \tag{12}$$

$$\|S\| = \sqrt{\tfrac{1}{2}S_{ij}S_{ij}}, \tag{13}$$

$$S_{ij} = \sigma_{ij} - \tfrac{1}{3}\delta_{ij}\sigma_{kk}. \tag{14}$$

Material constants for this viscoplastic constitutive formulation[19] for copper have the values: $A = 2\times10^7$ per second; $C = 13$ MPa; $n = 4.5$; $Q = 2\times10^5$ Joules/mol.; $R = 8.314$ Joules/(mol.$^\circ$ K); $T_m = 1356^\circ$ K; and $T_t = \frac{1}{2}T_m$.

The preceding equations represent a simple Norton creep law where no account is taken of the history dependence of the inelastic deformation behavior. This is adequate for the type of loading considered in this paper, but for more complicated loading conditions it is necessary to use some form of unified viscoplastic constitutive formulation[19] where history dependence is accounted for with internal state variables.

3 Numerical Solution of the Nonlinear Integral Equation

3.1 Solution Under Overall Strain Control

For two-dimensional fibrous composites the integral equation for $\Delta\varepsilon^{\mathrm{T}}_{kl}(\mathbf{r})$ reduces to the form

$$\begin{aligned}\Delta\varepsilon^{\mathrm{T}}_{kl}(\mathbf{r}) &= \Delta\varepsilon^{0}_{kl} + \frac{1}{A_c}\sum_{n_p=0}^{\pm\infty}{}' g_{klmn}(\zeta)\iint_{A_c} e^{i\boldsymbol{\xi}\cdot(\mathbf{r}-\mathbf{r}')}\left\{D^{\mathrm{m}}_{mnrs}\Delta c_{rs}(\mathbf{r}') - \right.\\ &\left. - \delta D_{mnrs}(\mathbf{r}')\left[\Delta\varepsilon^{\mathrm{T}}_{rs}(\mathbf{r}') - \Delta c_{rs}(\mathbf{r}')\right]\right\} dS(\mathbf{r}'), \end{aligned} \tag{15}$$

where $A_c = L_1 L_2$ is the area of the unit cell. Nemat-Nasser and his colleagues[4–9] and the authors[1–3] have demonstrated that good accuracy can be achieved by dividing the unit cell into a number of subvolumes, and by approximating the strain increment $\Delta\varepsilon^{\mathrm{T}}_{kl}(\mathbf{r}')$ in the βth subvolume integral with its average value in the subvolume, viz.,

$$\Delta\varepsilon^{\mathrm{T}}_{rs}(\mathbf{r}') \equiv \Delta\varepsilon^{\mathrm{T}\beta}_{rs} = \frac{1}{A_\beta}\iint_{A_\beta}\Delta\varepsilon^{\mathrm{T}}_{rs}(\mathbf{r})\, dS(\mathbf{r}'), \tag{16}$$

where A_β is the cross-sectional area of the subvolume.

Let there be N subvolumes in the unit cell, with M subvolumes in the fiber and $N - M$ subvolumes in the matrix. Then the preceding integral equation, with a piecewise constant strain approximation in the subvolume integral, can be written as

$$\begin{aligned}\Delta\varepsilon^{\mathrm{T}}_{kl}(\mathbf{r}) &= \Delta\varepsilon^{0}_{kl} + \frac{1}{A_c}\sum_{\beta=1}^{N}\sum_{n_p=0}^{\pm\infty}{}' g_{klmn}(\zeta)\, e^{i\boldsymbol{\xi}\cdot\mathbf{r}}\iint_{A_\beta} e^{-i\boldsymbol{\xi}\cdot\mathbf{r}'} dS(\mathbf{r}')\times\\ &\times\left\{D^{\mathrm{m}}_{mnrs}\Delta c^{\beta}_{rs} - \delta D^{\beta}_{mnrs}\left[\Delta\varepsilon^{\mathrm{T}\beta}_{rs} - \Delta c^{\beta}_{rs}\right]\right\}, \end{aligned} \tag{17}$$

where $\delta D^{\beta}_{mnrs} = D^{\mathrm{f}}_{mnrs} - D^{\mathrm{m}}_{mnrs}$ or 0, according as the subvolume β is in the fiber or matrix, respectively.

If we use Nemat-Nasser's notation and write

$$Q^{\alpha}(\boldsymbol{\xi}) = \frac{1}{A_\alpha}\iint_{A_\alpha} e^{i\boldsymbol{\xi}\cdot\mathbf{r}}\, dS(\mathbf{r}) \tag{18}$$

and denote

$$f^{\alpha} = \frac{A_{\alpha}}{A_c} \tag{19}$$

as the volume fraction of the αth subvolume, then the preceding equation may be written as

$$\Delta\varepsilon_{kl}^{\mathrm{T}}(\mathbf{r}) = \Delta\varepsilon_{kl}^{0} + \sum_{\beta=1}^{N}\sum_{n_p=0}^{\pm\infty}{}' g_{klmn}(\boldsymbol{\zeta})\, e^{i\boldsymbol{\xi}\cdot\mathbf{r}} f^{\beta} Q^{\beta}(-\boldsymbol{\xi}) \left\{ D^{\mathrm{m}}_{mnrs}\Delta c^{\beta}_{rs} - \delta D^{\beta}_{mnrs}\left[\Delta\varepsilon^{\mathrm{T}\beta}_{rs} - \Delta c^{\beta}_{rs}\right]\right\}. \tag{20}$$

We may now volume average equation (20) over the αth subvolume to obtain

$$\Delta\varepsilon_{kl}^{\mathrm{T}\alpha} = \Delta\varepsilon_{kl}^{0} + \sum_{\gamma=1}^{N} f^{\gamma} A^{\alpha\gamma}_{klrs}\Delta c^{\gamma}_{rs} - \sum_{\beta=1}^{M} f^{\beta} S^{\alpha\beta}_{klrs}\Delta\varepsilon^{\mathrm{T}\beta}_{rs}, \tag{21}$$

where

$$S^{\alpha\beta}_{klrs} = \sum_{n_p=0}^{\pm\infty}{}' g_{klmn}(\boldsymbol{\zeta})\, \delta D^{\beta}_{mnrs} Q^{\alpha}(\boldsymbol{\xi})\, Q^{\beta}(-\boldsymbol{\xi}) \tag{22}$$

and

$$A^{\alpha\beta}_{klrs} = S^{\alpha\beta}_{klrs} + \sum_{n_p=0}^{\pm\infty}{}' g_{klmn}(\boldsymbol{\zeta})\, D^{\mathrm{m}}_{mnrs} Q^{\alpha}(\boldsymbol{\xi})\, Q^{\beta}(-\boldsymbol{\xi}). \tag{23}$$

The matrix tensors $A^{\alpha\beta}_{klrs}$ and $S^{\alpha\beta}_{klrs}$ are akin to Eshelby's[10,11] tensor for an ellipsoidal inclusion, but account for the interaction of the fiber with its neighbors in the infinite lattice. It may be noted that the last term in equation (21) is summed only over the subvolumes in the fiber, where $(1 \le \beta \le M)$, since $\delta D^{\beta}_{mnrs} = 0$ if the βth subvolume resides in the matrix, so that

$$S^{\alpha\beta}_{klrs} = 0 \quad \text{for} \quad M < \beta \le N. \tag{24}$$

Thus only M unknowns (associated with the subvolumes in the fiber) are involved in equation (21). When this relation is assembled columnwise for each subvolume α, the solution to the $6M \times 6M$ system of equations can be obtained by LU decomposition. We then have to solve the system of equations

$$\sum_{\beta=1}^{M} B^{\alpha\beta}_{klrs}\Delta\varepsilon^{\mathrm{T}\beta}_{rs} = \Delta b^{\alpha}_{kl} \quad \text{for} \quad \alpha = 1, 2, \ldots, M \tag{25}$$

where

$$B^{\alpha\beta}_{klrs} = \delta^{\alpha\beta} I_{klrs} + f^{\beta} S^{\alpha\beta}_{klrs}, \tag{26}$$

with $I_{klrs} = (\delta_{kr}\delta_{ls} + \delta_{ks}\delta_{lr})/2$ denoting the fourth rank identity tensor, $\delta^{\alpha\beta}$ the matrix Kronecker delta, and

$$\Delta b^{\alpha}_{kl} = \Delta\varepsilon^{0}_{kl} + \sum_{\gamma=1}^{N} f^{\gamma} A^{\alpha\gamma}_{klrs}\Delta c^{\gamma}_{rs}. \tag{27}$$

Equation (21) can then be used with the known values of $\Delta\varepsilon_{kl}^{\mathrm{T}\beta}$ in the fiber subvolumes, where $(1 \leq \beta \leq M)$, to compute the values of $\Delta\varepsilon_{kl}^{\mathrm{T}\alpha}$ in the matrix subvolumes, where $(M < \alpha \leq N)$.

An explicit solution for the total strain increment can be found from equation (25) if the total strain increment is small. Under these circumstances the inelastic strain increment can be computed explicitly from equation (10) in the Euler forward difference form,

$$\Delta\varepsilon_{ij}^{\mathrm{P}} = \tfrac{1}{2}\|\dot{\boldsymbol{\varepsilon}}^{\mathrm{P}}\|\frac{S_{ij}}{\|\boldsymbol{S}\|}\,\Delta t. \tag{28}$$

In this form the inelastic strain increment is independent of the total strain increment and the right hand side vector Δb_{kl}^{α} in equation (25) can be evaluated from equations (2), (27) and (28). However, if an implicit scheme such as backward Euler integration (or a forward difference subincrementation method) is used to evaluate the inelastic strain increment, then $\Delta\varepsilon_{ij}^{\mathrm{P}}$ will depend on $\Delta\varepsilon_{kl}^{\mathrm{T}}$ and equation (25) must be used iteratively to solve for $\Delta\varepsilon_{kl}^{\mathrm{T}}$, i.e.

$$\sum_{\beta=1}^{M} B_{klrs}^{\alpha\beta}\left\{\Delta\varepsilon_{rs}^{\mathrm{T}\beta}\right\}_{\lambda+1} = \Delta b_{kl}^{\alpha}\left(\left\{\Delta\varepsilon_{pq}^{\mathrm{T}\gamma}\right\}_{\lambda}\right) \quad \text{for} \quad \left\{\begin{array}{l}\alpha = 1,2,\ldots,M\\ \gamma = 1,2,\ldots,N\end{array}\right\} \tag{29}$$

where λ is the iteration number.

Once the values of $\Delta\varepsilon_{kl}^{\mathrm{T}\alpha}$ have been determined, further resolution can be obtained, if required, from equation (20). By substituting different $\mathbf{r}$ values in this equation we may evaluate $\Delta\varepsilon_{kl}^{\mathrm{T}}(\mathbf{r})$ at any point within a subvolume. However, the Fourier series solution in (20) will exhibit Gibbs' phenomenon, in which the solution oscillates spatially with $\mathbf{r}$ near the fiber/matrix interface. These oscillations have a period[20] of L_γ/N_γ for $\gamma = 1,2$ where L_γ is the length of the unit cell and N_γ is the number of terms in the Fourier summation corresponding to the γth direction. It is therefore appropriate to average equation (20) over a small rectangular area about the point $\mathbf{r}$. This results in the term $e^{i\boldsymbol{\xi}\cdot\mathbf{r}}$ being replaced with the Laue interference integral, $Q^{\alpha}(\boldsymbol{\xi})$, for a small rectangular subvolume[3] of dimensions $L_1/N_1 \times L_2/N_2$.

3.2 Solution Under Overall Stress Control

In the preceding section the equations governing the total strain increment distribution in the unit cell were derived under the assumption that the composite was subjected to a uniform overall strain increment given by $\Delta\varepsilon_{ij}^{0}$. When a uniform overall stress increment, $\Delta\sigma_{ij}^{0}$, is applied to the composite, it is necessary to obtain $\Delta\varepsilon_{ij}^{0}$ as a function of $\Delta\sigma_{ij}^{0}$.

The overall stress and strain increments are equated to the volume averages of $\Delta\sigma_{ij}(\mathbf{r})$ and $\Delta\varepsilon_{ij}^{\mathrm{T}}(\mathbf{r})$ over the unit periodic cell. Hence, for fibrous composites, equation (1) can be volume

averaged over the unit cell to give

$$\Delta\sigma_{ij}^{0} = \frac{1}{A_c}\iint\limits_{A_c} D_{ijkl}\left(\mathbf{r}\right)\left(\Delta\varepsilon_{kl}^{\mathrm{T}}\left(\mathbf{r}\right) - \Delta c_{kl}\left(\mathbf{r}\right)\right)\, dS(\mathbf{r}). \tag{30}$$

When equation (3) is substituted into the preceding equation and we replace $\Delta\varepsilon_{kl}^{\mathrm{T}}\left(\mathbf{r}\right)$ and $\Delta c_{kl}\left(\mathbf{r}\right)$ with their discretized subvolume counterparts, we obtain

$$\Delta\sigma_{ij}^{0} = \lambda^{\mathrm{m}}\delta_{ij}\Delta\varepsilon_{kk}^{0} + 2\mu^{\mathrm{m}}\Delta\varepsilon_{ij}^{0} + \Delta R_{ij} + \Delta T_{ij}, \tag{31}$$

in which

$$\Delta R_{ij} = \sum_{\beta=1}^{M} f^{\beta}\left[\left(\lambda^{\beta} - \lambda^{\mathrm{m}}\right)\delta_{ij}\Delta\varepsilon_{kk}^{\mathrm{T}\beta} + 2\left(\mu^{\beta} - \mu^{\mathrm{m}}\right)\Delta\varepsilon_{ij}^{\mathrm{T}\beta}\right] \tag{32}$$

and

$$\Delta T_{ij} = -\sum_{\gamma=1}^{N} f^{\gamma}\left(\lambda^{\gamma}\delta_{ij}\Delta c_{kk}^{\gamma} + 2\mu^{\gamma}\Delta c_{ij}^{\gamma}\right). \tag{33}$$

In the preceding equations isotropic relations have been assumed for D_{ijkl}^{β} and δD_{ijkl}^{β} in the form

$$D_{ijkl}^{\beta} = \lambda^{\beta}\delta_{ij}\delta_{kl} + \mu^{\beta}\left(\delta_{ik}\delta_{jl} + \delta_{il}\delta_{jk}\right) \tag{34}$$

and

$$\delta D_{ijkl}^{\beta} = \left(\lambda^{\beta} - \lambda^{\mathrm{m}}\right)\delta_{ij}\delta_{kl} + \left(\mu^{\beta} - \mu^{\mathrm{m}}\right)\left(\delta_{ik}\delta_{jl} + \delta_{il}\delta_{jk}\right), \tag{35}$$

where the superscript $\beta = \mathrm{f}$ or m, according as the βth subvolume is in the fiber or matrix, respectively.

Equation (31) can be inverted to give

$$\Delta\varepsilon_{ij}^{0} = \frac{\Delta\sigma_{ij}^{0} - \Delta R_{ij} - \Delta T_{ij}}{2\mu^{\mathrm{m}}} - \delta_{ij}\frac{\lambda^{\mathrm{m}}}{2\mu^{\mathrm{m}}\left(3\lambda^{\mathrm{m}} + 2\mu^{\mathrm{m}}\right)}\left(\Delta\sigma_{kk}^{0} - \Delta R_{kk} - \Delta T_{kk}\right). \tag{36}$$

This may now be substituted into the integral equation (21), and when all the terms containing $\Delta\varepsilon_{kl}^{\mathrm{T}\alpha}$ are taken over to the left hand side, the system of equations takes the form

$$\sum_{\beta=1}^{M} C_{klrs}^{\alpha\beta}\Delta\varepsilon_{rs}^{\mathrm{T}\beta} = \Delta a_{kl}^{\alpha} \quad \text{for} \quad \alpha = 1, 2, \ldots, M \tag{37}$$

where

$$\begin{aligned} C_{klrs}^{\alpha\beta} \;=\; & \delta^{\alpha\beta}I_{klrs} + f^{\beta}S_{klrs}^{\alpha\beta} + \frac{f^{\beta}}{2\mu^{\mathrm{m}}}\left\{\left(\lambda^{\beta} - \lambda^{\mathrm{m}}\right)\delta_{kl}\delta_{rs} + 2\left(\mu^{\beta} - \mu^{\mathrm{m}}\right)I_{klrs}\right\} - \\ & - f^{\beta}\frac{\lambda^{\mathrm{m}}}{2\mu^{\mathrm{m}}\left(3\lambda^{\mathrm{m}} + 2\mu^{\mathrm{m}}\right)}\left\{3\left(\lambda^{\beta} - \lambda^{\mathrm{m}}\right) + 2\left(\mu^{\beta} - \mu^{\mathrm{m}}\right)\right\}\delta_{kl}\delta_{rs} \end{aligned} \tag{38}$$

and

$$\Delta a_{kl}^{\alpha} = \frac{\Delta\sigma_{kl}^{0} - \Delta T_{kl}}{2\mu^{\mathrm{m}}} - \delta_{kl}\frac{\lambda^{\mathrm{m}}}{2\mu^{\mathrm{m}}\left(3\lambda^{\mathrm{m}} + 2\mu^{\mathrm{m}}\right)}\left(\Delta\sigma_{pp}^{0} - \Delta T_{pp}\right) + \sum_{\gamma=1}^{N} f^{\gamma} A_{klrs}^{\alpha\gamma}\Delta c_{rs}^{\gamma}. \tag{39}$$

When equation (37) is solved for $\Delta\varepsilon_{rs}^{\mathrm{T}\beta}$ for all the subvolumes in the fiber, ΔR_{ij} may be evaluated from (32) and substituted into (36) to obtain the overall strain increment, $\Delta\varepsilon_{ij}^{0}$. Equation (21) is then available to determine $\Delta\varepsilon_{kl}^{\mathrm{T}\alpha}$ in every subvolume in the unit cell.

3.3 Matrix Assembly of Discretized Integral Equation

The solution of the integral equation in (25) requires the evaluation of the matrix tensors $S_{klrs}^{\alpha\beta}$ and $A_{klrs}^{\alpha\beta}$ from equations (22) and (23). For isotropic constituents the matrix tensor $S_{klrs}^{\alpha\beta}$ involves the evaluation of $g_{klmn}(\boldsymbol{\zeta})\,\delta D_{mnrs}^{\beta}$, which may be written from (6) and (7) in the form

$$\begin{aligned} g_{klmn}(\boldsymbol{\zeta})\,\delta D_{mnrs}^{\beta} = \quad & \left(\frac{\lambda^{\beta} - \lambda^{\mathrm{m}}}{\lambda^{\mathrm{m}}}\right)\left(\frac{\lambda^{\mathrm{m}}}{\lambda^{\mathrm{m}} + 2\mu^{\mathrm{m}}}\right)\delta_{rs}\zeta_k\zeta_l + \\ & + \left(\frac{\mu^{\beta} - \mu^{\mathrm{m}}}{2\mu^{\mathrm{m}}}\right)\left(\delta_{rk}\zeta_s\zeta_l + \delta_{ks}\zeta_r\zeta_l + \delta_{lr}\zeta_s\zeta_k + \delta_{ls}\zeta_r\zeta_k\right) - \\ & - 2\left(\frac{\mu^{\beta} - \mu^{\mathrm{m}}}{\mu^{\mathrm{m}}}\right)\left(\frac{\lambda^{\mathrm{m}} + \mu^{\mathrm{m}}}{\lambda^{\mathrm{m}} + 2\mu^{\mathrm{m}}}\right)\zeta_r\zeta_s\zeta_k\zeta_l, \end{aligned} \tag{40}$$

where $\lambda^{\beta}, \mu^{\beta}$ and $\lambda^{\mathrm{m}}, \mu^{\mathrm{m}}$ are the Lamé constants for the βth subvolume and the matrix, and

$$\zeta_i = \frac{\xi_i}{\sqrt{\left(2\pi n_1/L_1\right)^2 + \left(2\pi n_2/L_2\right)^2}} \quad \text{for} \quad i = 1, 2. \tag{41}$$

with $\xi_1 = 2\pi n_1/L_1$, $\xi_2 = 2\pi n_2/L_2$. The assembly of the matrix tensor $A_{klrs}^{\alpha\beta}$ requires the evaluation of $g_{klmn}(\boldsymbol{\zeta})\,D_{mnrs}^{\mathrm{m}}$, and this is obtained by replacing $\lambda^{\beta} - \lambda^{\mathrm{m}}$ and $\mu^{\beta} - \mu^{\mathrm{m}}$ in equation (40) with λ^{m} and μ^{m}, respectively.

In the preceding derivation the isotropic form of equation (7),

$$M_{ij}(\boldsymbol{\zeta}) = \mu^{\mathrm{m}}\delta_{ij} + \left(\lambda^{\mathrm{m}} + \mu^{\mathrm{m}}\right)\zeta_i\zeta_j, \tag{42}$$

with inverse

$$M_{ij}^{-1}(\boldsymbol{\zeta}) = \frac{\delta_{ij}}{\mu^{\mathrm{m}}} - \frac{\lambda^{\mathrm{m}} + \mu^{\mathrm{m}}}{\mu^{\mathrm{m}}\left(\lambda^{\mathrm{m}} + 2\mu^{\mathrm{m}}\right)}\zeta_i\zeta_j, \tag{43}$$

obtained by substituting (34) into (7), is used. Substitution of (43) into (6) together with the use of (35) then yields the relationship given in (40).

The remaining factor required for assembling the matrix tensors $S_{klrs}^{\alpha\beta}$ and $A_{klrs}^{\alpha\beta}$ is the Laue interference product, $Q^{\alpha}(\boldsymbol{\xi})\,Q^{\beta}(-\boldsymbol{\xi})$, with $Q^{\alpha}(\boldsymbol{\xi})$ defined by equation (18) in which A_{α} denotes the area of the αth triangular subvolume.

Let the vertices of the αth triangular subvolume have coordinates (x_1^α, y_1^α), (x_2^α, y_2^α), (x_3^α, y_3^α). We map the Cartesian coordinate system (x, y) into a new system (r, s), in which the vertices of the mapped triangle are at the points $(0,0)$, $(1,0)$, $(0,1)$. This mapping is accomplished with the relationships

$$x = x_1^\alpha + (x_2^\alpha - x_1^\alpha)\, r + (x_3^\alpha - x_1^\alpha)\, s \tag{44}$$

and

$$y = y_1^\alpha + (y_2^\alpha - y_1^\alpha)\, r + (y_3^\alpha - y_1^\alpha)\, s. \tag{45}$$

The area transforms according to the usual Jacobian relation $dx\, dy = J\,(r, s)\; dr\, ds$, in which

$$\begin{aligned} J\,(r,s) &= \frac{\partial\,(x,y)}{\partial\,(r,s)} = \begin{vmatrix} \dfrac{\partial x}{\partial r} & \dfrac{\partial y}{\partial r} \\ \dfrac{\partial x}{\partial s} & \dfrac{\partial y}{\partial s} \end{vmatrix} = \begin{vmatrix} x_2^\alpha - x_1^\alpha & y_2^\alpha - y_1^\alpha \\ x_3^\alpha - x_1^\alpha & y_3^\alpha - y_1^\alpha \end{vmatrix} \\ &= (x_2^\alpha - x_1^\alpha)(y_3^\alpha - y_1^\alpha) - (x_3^\alpha - x_1^\alpha)(y_2^\alpha - y_1^\alpha) = 2A_\alpha, \end{aligned} \tag{46}$$

and where the last equality is obtained by means of the identity,

$$\iint\limits_{A_\alpha} dx\, dy = \int_{s=0}^{1} \int_{r=0}^{1-s} J\,(r,s)\; dr\, ds = \frac{1}{2} \frac{\partial\,(x,y)}{\partial\,(r,s)} = A_\alpha. \tag{47}$$

The Laue interference integral can now be written as

$$\begin{aligned} Q^\alpha(\boldsymbol{\xi}) &= \frac{1}{A_\alpha} \iint\limits_{A_\alpha} e^{i(\xi_1 x + \xi_2 y)}\, dx\, dy \\ &= \frac{1}{A_\alpha} \int_{s=0}^{1} \int_{r=0}^{1-s} e^{i\left\{\xi_1\left[x_1^\alpha + \left(x_2^\alpha - x_1^\alpha\right) r + \left(x_3^\alpha - x_1^\alpha\right) s\right] + \xi_2\left[y_1^\alpha + \left(y_2^\alpha - y_1^\alpha\right) r + \left(y_3^\alpha - y_1^\alpha\right) s\right]\right\}} \frac{\partial\,(x,y)}{\partial\,(r,s)}\, dr\, ds \\ &= 2 \int_{s=0}^{1} \int_{r=0}^{1-s} e^{i\left\{\xi_1\left[x_1^\alpha + \left(x_2^\alpha - x_1^\alpha\right) r + \left(x_3^\alpha - x_1^\alpha\right) s\right] + \xi_2\left[y_1^\alpha + \left(y_2^\alpha - y_1^\alpha\right) r + \left(y_3^\alpha - y_1^\alpha\right) s\right]\right\}}\, dr\, ds. \end{aligned} \tag{48}$$

After the integration is performed, the relations for $Q^\alpha(\boldsymbol{\xi})$ and $Q^\beta(-\boldsymbol{\xi})$ can be separated into their real and imaginary components, yielding

$$Q^\alpha(\boldsymbol{\xi}) = Q_1^\alpha(\xi_1, \xi_2) + i Q_2^\alpha(\xi_1, \xi_2) \tag{49}$$

and

$$Q^\beta(-\boldsymbol{\xi}) = Q_1^\beta(\xi_1, \xi_2) - i Q_2^\beta(\xi_1, \xi_2). \tag{50}$$

In evaluating the Laue product $Q^\alpha(\boldsymbol{\xi}) Q^\beta(-\boldsymbol{\xi})$, we need retain only the real part, since the imaginary part vanishes on summing over n_1, n_2 in the Fourier expansion. Accordingly, we may write

$$Q^\alpha(\boldsymbol{\xi}) Q^\beta(-\boldsymbol{\xi}) = Q_1^\alpha(\xi_1, \xi_2) Q_1^\beta(\xi_1, \xi_2) + Q_2^\alpha(\xi_1, \xi_2) Q_2^\beta(\xi_1, \xi_2). \tag{51}$$

On integration, equation (48) yields the relations,

$$Q_1^\alpha(\xi_1,\xi_2) = 2\left(\frac{\cos\left(\xi_1 x_2^\alpha + \xi_2 y_2^\alpha\right)}{\left(\xi_1(x_1^\alpha - x_2^\alpha) + \xi_2(y_1^\alpha - y_2^\alpha)\right)\left(\xi_1(x_2^\alpha - x_3^\alpha) + \xi_2(y_2^\alpha - y_3^\alpha)\right)} - \right.$$
$$- \frac{\cos\left(\xi_1 x_1^\alpha + \xi_2 y_1^\alpha\right)}{\left(\xi_1(x_1^\alpha - x_2^\alpha) + \xi_2(y_1^\alpha - y_2^\alpha)\right)\left(\xi_1(x_1^\alpha - x_3^\alpha) + \xi_2(y_1^\alpha - y_3^\alpha)\right)} -$$
$$\left. - \frac{\cos\left(\xi_1 x_3^\alpha + \xi_2 y_3^\alpha\right)}{\left(\xi_1(x_1^\alpha - x_3^\alpha) + \xi_2(y_1^\alpha - y_3^\alpha)\right)\left(\xi_1(x_2^\alpha - x_3^\alpha) + \xi_2(y_2^\alpha - y_3^\alpha)\right)}\right) \qquad (52)$$

and

$$Q_2^\alpha(\xi_1,\xi_2) = 2\left(\frac{\sin\left(\xi_1 x_2^\alpha + \xi_2 y_2^\alpha\right)}{\left(\xi_1(x_1^\alpha - x_2^\alpha) + \xi_2(y_1^\alpha - y_2^\alpha)\right)\left(\xi_1(x_2^\alpha - x_3^\alpha) + \xi_2(y_2^\alpha - y_3^\alpha)\right)} - \right.$$
$$- \frac{\sin\left(\xi_1 x_1^\alpha + \xi_2 y_1^\alpha\right)}{\left(\xi_1(x_1^\alpha - x_2^\alpha) + \xi_2(y_1^\alpha - y_2^\alpha)\right)\left(\xi_1(x_1^\alpha - x_3^\alpha) + \xi_2(y_1^\alpha - y_3^\alpha)\right)} -$$
$$\left. - \frac{\sin\left(\xi_1 x_3^\alpha + \xi_2 y_3^\alpha\right)}{\left(\xi_1(x_1^\alpha - x_3^\alpha) + \xi_2(y_1^\alpha - y_3^\alpha)\right)\left(\xi_1(x_2^\alpha - x_3^\alpha) + \xi_2(y_2^\alpha - y_3^\alpha)\right)}\right). \qquad (53)$$

The relations for $Q_1^\beta(\xi_1,\xi_2)$ and $Q_2^\beta(\xi_1,\xi_2)$ are the same as the preceding relations with β substituted for α.

In the case of rectangular subvolumes we have shown[3] that the Laue interference integral contains products of the function $\sin x/x$ and it is necessary to attend to the limiting case where the denominator $x \to 0$ and $\sin x/x \to 1 \quad \text{as} \quad x \to 0$. For triangular subvolumes the denominators in the Laue interference integrals in (52) and (53) vanish under nine separate circumstances, and the limiting form of the integrals, $Q_1^\alpha(\xi_1,\xi_2)$ and $Q_2^\alpha(\xi_1,\xi_2)$, are given in the Appendix. The confluent case where ξ_1 and ξ_2 are both zero is of no concern, since this case is excluded from the Fourier summation.

In the limiting forms given in the Appendix, it is assumed that the denominators are exactly zero. When, for example, the denominators are nonzero but small, it is necessary to expand equations (52) and (53) into a Taylor series in ascending powers of the small quantities for the nine cases. This can easily be achieved with the aid of a symbolic algebra software package.

4 Numerical Examples

Bahei-El-Din, Dvorak and their colleagues[21,22] have given cogent arguments which show that it is inappropriate to assume that the stress and strain increments in the unit cell are spatially uniform in

each phase of the composite. They found that when the true (within discretization error) stress and strain increments in the unit cell were calculated throughout the loading history and the results were volume averaged to produce the overall macroscopic response, the results were significantly different from those (e.g. self-consistent and Mori-Tanaka schemes) in which the overall macroscopic response was found by assuming spatially constant fields in each phase. This was found to be especially true in composites loaded into the plastic region where the constitutive material properties vary at each point in the unit cell in accordance with the spatially varying field histories. In the preceding studies the true field histories in the unit cell were obtained with the use of a periodic hexagonal array model[23] in which periodic boundary conditions were applied to a finite element discretization of the unit cell.

Aboudi and his colleagues[24–26] have also examined the field histories within the unit cell of a periodic composite by discretizing the unit cell into rectangular subvolumes and by enforcing periodicity through continuity of displacements and surface tractions at the unit cell boundary.

Both of the preceding methods employ a field theory approach in which the deformation behavior within a subvolume depends only on the displacements and tractions at its surface. Here, we study the field histories by discretizing the unit cell into triangular subvolumes, and periodicity is enforced naturally by expanding the field histories into Fourier series. Since an integral equation scheme is adopted, the method is an "action at a distance" approach in which the deformation behavior within a subvolume depends on the field histories in all the other subvolumes comprising the composite material. The Fourier series method essentially restricts the interaction between the subvolumes to those within the unit cell, whilst the Green's function approach[1–3,28] requires the interaction to be evaluated between all subvolumes in the composite, though the interaction is strong only for a subvolume which interacts with the subvolumes in its own and neighboring unit cells in the periodic lattice.

The size of the matrix which must be solved by LU decomposition for a fiber with M subvolumes is $6M \times 6M$. If the fiber has a square planform with n subvolumes along each side, then the size of the matrix increases with the number of subvolumes along a side according to $36n^4$. For a three-dimensional cuboidal inclusion the size of the matrix increases as $36n^6$, so that a three-dimensional problem has a matrix size n^2 times as big as that for a corresponding two-dimensional problem.

In order to demonstrate that the triangular subvolume approach gives reliable results, we first calculate the result of elastically loading a fibrous metal matrix composite. Figure 1 shows the transverse stresses, σ_{11}, in each subvolume within the unit periodic cell, when a W/Cu fibrous composite is loaded in the transverse direction with an overall uniform stress of $\sigma^0_{11} = 1000$ kPa.

The tungsten fiber is assumed to be of square planform and occupies a volume fraction of $f = 9/49 = 0.184$ in the unit cell of the composite, with $E_{\rm W} = 395$ GPa, $\nu_{\rm W} = 0.28$, $E_{\rm Cu} = 127$ GPa and $\nu_{\rm Cu} = 0.34$. Fig. 1(a) presents a numerical tabulation of the constant-valued stresses for each of the 49 square subvolumes, using the Laue interference product, $Q^{\alpha}(\boldsymbol{\xi})\, Q^{\beta}(-\boldsymbol{\xi})$, for rectangular subvolumes presented in a previous paper[3]. The corresponding results when the unit cell is discretized with triangular subvolumes is presented in Fig. 1(b), where it may be seen that the cell is discretized with the hypotenuse of each triangle biased in the northeast direction. This causes slight asymmetries in the resultant elastic stress distribution within the unit cell. However, when the results from the two triangular subvolumes in Fig. 1(b)—into which each rectangular subvolume in Fig. 1(a) is broken—are averaged, the results in the two figures agree very closely. These results were obtained by summing the Fourier series to $n_p = \pm 200$ for $p = 1, 2$ in equations (22) and (23). The results do not differ significantly from those obtained by summing the series to $n_p = \pm 50$.

We now consider the W/Cu composite as an assemblage of unit cells in which the tungsten fiber is assumed to be elastic whilst the copper matrix is assumed to be a ductile viscoplastic material whose inelastic response is governed by equations (10)–(14). The triangular discretization of the unit cell is shown in Fig. 1(b). Another discretization, in which the hypotenuse of each triangle is biased in the northwest direction, was also used and the subvolume stresses were averaged to eliminate asymmetries due to meshing.

The composite is loaded in the transverse direction under overall stress control at a stress rate of $\dot{\sigma}^0_{11} = 10$ MPa per second to a maximum overall stress of $\sigma^0_{11} = 100$ MPa at a temperature of 814° K or $0.6T_m$. It is then allowed to creep at this overall stress for 3600 seconds, and is then unloaded to an overall stress of $\sigma^0_{11} = 0$ MPa at an overall stress rate of $\dot{\sigma}^0_{11} = -10$ MPa per second. All other components of $\dot{\sigma}^0_{ij}$ other than $\dot{\sigma}^0_{11}$ are taken to be zero.

Figure 2(a) shows the transverse stresses, σ_{11}, within the unit cell at the end of the initial 10 second loading when the overall stress is $\sigma^0_{11} = 100$ MPa. Stresses are rounded to the nearest integer. The numerical tabulation in Fig. 2(a) is presented as a topological map in Fig. 2(b), where the height represents the magnitude of the transverse stress concentration factors. The transverse stress distribution forms a ridged valley where the stress gradient parallel to the loading direction is relatively small, and where the stress is higher in the ridges near the north and south fiber/matrix interfaces and is smaller in the valley which runs parallel to the loading direction in the center of the fiber. The formation of a ridged valley is due to the assumed square shape of the tungsten fiber, and to a lesser extent, to the interaction between the neighboring fibers in the periodic lattice. A

similar ridged valley is observed when a cuboidal fiber embedded in an infinite matrix experiences a uniform eigenstrain[11].

Figure 3(a) shows a tabulation of the local hydrostatic stress field, $(\sigma_{11} + \sigma_{22} + \sigma_{33})/3$, for the same transverse loading condition. High hydrostatic stresses occur at the fiber/matrix interface perpendicular to the direction of the loading axis, and Fig. 3(b) shows the results as a topological map.

The transverse stresses within the unit cell after one hour of creep are shown in Figs 4(a) and 4(b). High stress gradients are present at the fiber/matrix interface and creep has the effect of increasing the heterogeneity within the unit cell in both the fiber and the matrix phases. On examining the hydrostatic stresses in Figs 5(a) and 5(b), we observe that some parts of the fiber are in hydrostatic tension whilst others are in hydrostatic compression. The matrix is in a state of hydrostatic tension with very large values observed at the fiber/matrix interface perpendicular to the loading axis.

After the composite is unloaded to a zero overall stress state, we see from Figs 6(a) and 6(b) that a high degree of residual transverse stress heterogeneity exists within the unit cell with relatively large tensile stresses in the ridges and compressive stresses in the central ridged valley of the fiber. The hydrostatic stresses in Figs 7(a) and 7(b) show a similar heterogeneous trend, with large compressive hydrostatic stresses in the fiber's central valley and smaller compressive hydrostatic stresses in the ridges. In the copper matrix, the tensile hydrostatic stress adjacent to the fiber/matrix interface perpendicular to the loading axis is about as large as that which would obtain by tranversely loading a uniform matrix material to 100 MPa.

As Dvorak has aptly remarked[22], these results serve as a salutory reminder that large errors can be obtained in homogenization techniques which employ the assumption that stress and strain distributions are homogeneous in each constituent phase of the composite under inelastic loading conditions.

5 Conclusions

This paper presents one of three known methods for analyzing the heterogeneous deformation behavior in the unit cell of an infinite periodic lattice when subjected to a uniform applied stress or strain loading increment. An integral equation approach is used to determine the total strain increment at any point in the unit cell. The integral equation is solved by a Fourier series expansion of the field variables and their spatial variations within the unit cell are approximated by a piecewise

constant distribution. Other approaches which have been considered in the literature are Aboudi's method of cells[24–26], the finite element method with periodic boundary conditions[21–23], and boundary element methods[27]. The inelastic stress distribution in the unit cell of a W/Cu metal matrix composite is evaluated when subjected to an overall transverse loading history imposed at a constant overall stress rate. The stress distribution in the unit cell is found to be very heterogeneous with the heterogeneity increasing with continued inelastic deformation in both the fully loaded and the unloaded condition.

6 Acknowledgements

The work of two of the authors (KPW and EHJ) was supported by the United States Department of Energy under Grant Number DE–FG02–92ER14247. Dr. Oscar P. Manley served as contract monitor.

References

[1] Walker, K.P., Jordan, E.H. & Freed, A.D., Nonlinear Mesomechanics of Composites With Periodic Microstructure: First Report. NASA TM-102051, 1989.

[2] Walker, K.P., Jordan, E.H. & Freed, A.D., Equivalence of Green's Function and the Fourier Series Representation of Composites With Periodic Microstructure, *Micromechanics and Inhomogeneity—The Toshio Mura Anniversary Volume.* Springer–Verlag, 535–558, 1990.

[3] Walker, K.P., Freed, A.D. & Jordan, E.H., Microstress Analysis of Periodic Composites. *Composites Engineering*, **1** No. 1 (1991) 29–40.

[4] Nemat-Nasser, S. & Taya, M., On Effective Moduli of an Elastic Body Containing Periodically Distributed Voids. *Quart. Appl. Math.*, **39** (1981) 43–59.

[5] Nemat-Nasser, S., Iwakuma, T. & Hejazi, M., On Composites with Periodic Structure. *Mechanics of Materials*, **1** (1982) 239–267.

[6] Nemat-Nasser, S. & Iwakuma, T., Micromechanically Based Constitutive Relations for Polycrystalline Solids. NASA CP 2271, 1983, pp. 113–136.

[7] Iwakuma, T. & Nemat-Nasser, S., Composites with Periodic Microstructure. *Computers and Structures*, **16** Nos. 1–4 (1983) 13–19.

[8] Accorsi, M.L. & Nemat-Nasser, S., Bounds on the Overall Elastic and Instantaneous Moduli of Periodic Composites. *Mechanics of Materials*, **5** (1986) 209–220.

[9] Nemat-Nasser, S., Iwakuma, T. & Accorsi, M., Cavity Growth and Grain Boundary Sliding in Polycrystalline Solids. *Mechanics of Materials*, **5** (1986) 317–329.

[10] Eshelby, J.D., The Determination of the Elastic Field of an Ellipsoidal Inclusion, and Related Problems. *Proc. Roy. Soc. London*, **A241** (1957) 376–396.

[11] Mura, T., *Micromechanics of Defects in Solids*, 2nd edition. Martinus-Nijhoff, Dordrecht, 1987.

[12] Barnett, D.M. & Swanger, L.A., The Elastic Energy of a Straight Dislocation in an Infinite Anisotropic Elastic Medium. *Phys. Stat. Sol. (b)*, **48** (1971) 419–428.

[13] Barnett, D.M., The Precise Evaluation of Derivatives of the Anisotropic Elastic Green's Functions. *Phys. Stat. Sol. (b)*, **49** (1972) 741–748.

[14] Gubernatis, J.E. & Krumhansl, J.A., Macroscopic Engineering Properties of Polycrystalline Materials: Elastic Properties. *Journal of Applied Physics*, **46** No. 5 (1975) 1875–1883.

[15] Korringa, K., Theory of Elastic Constants of Heterogeneous Media. *J. Math. Phys.*, **14** No. 4 (1973) 509–513.

[16] Zeller, R. & Dederichs, P.H., Elastic Constants of Polycrystals. *Phys. Stat. Sol. (b)*, **55** (1973) 831–842.

[17] Levin, V.M., Determination of Composite Material Elastic and Thermoelastic Constants. *Isv. AN SSSR, Mekhanika Tverdogo Tela*, **11** No. 6 (1976) 137–145.

[18] Chen, F.C. & Young, K., Inclusions of Arbitrary Shape in an Elastic Medium. *J. Math. Phys.*, **18** No. 7 (1977) 1412–1416.

[19] Freed, A.D. & Walker, K.P., Viscoplasticity with Creep and Plasticity Bounds, submitted to *International Journal of Plasticity*, 1992.

[20] Carslaw, H.S., *An Introduction to the Theory of Fourier's Series and Integrals*, Chapter IX, Third Revised Edition, Dover Publications, Inc., New York, 1950.

[21] Bahei-El-Din, Y.A., Dvorak, G.J., Lin, J., Shah, R. & Wu, J.F., Local Fields and Overall Response of Fibrous and Particulate Metal Matrix Composites. Final Technical Report to Alcoa Laboratories on Contract 379(52R)053(22L), Rensselaer Polytechnic Institute, Troy, NY 12180, 1987.

[22] Dvorak, G.J., Plasticity Theories for Fibrous Composite Materials, *Metal Matrix Composites: Mechanisms and Properties*, edited by R.K. Everett and R.J. Arsenault, Academic Press, Boston, 1991, pp. 1–77.

[23] Teply, J.L. & Dvorak, G.J., Bounds on Overall Instantaneous Properties of Elastic-Plastic Composites. *J. Mech. Phys. Solids*, **5** (1988) 29–58.

[24] Aboudi, J., Micromechanical Analysis of Composites by the Method of Cells, *Appl. Mech. Rev.*, **42** (1989) 193–221.

[25] Aboudi, J., *Mechanics of Composite Materials—A Unified Micromechanical Approach.* Elsevier, Amsterdam, 1991.

[26] Paley, M. & Aboudi, J., Micromechanical Analysis of Composites by the Generalized Cells Model, submitted to *Mechanics of Materials*, 1992.

[27] Banerjee, P.K. & Henry, D.P., Elastic Analysis of Three-Dimensional Solids with Fiber Inclusions by BEM, *Int. J. Solids Structures*, in press, 1992.

[28] Walker, K.P., Freed, A.D. & Jordan, E.H., Accuracy of the Generalized Self-Consistent Method in Modelling the Elastic Behavior of Periodic Composites, submitted to *Proc. Roy. Soc. London*, 1992.

7 Appendix

Case 1: $y_3^\alpha = y_1^\alpha$ and $\xi_1 = 0$

$$Q_1^\alpha(\xi_1,\xi_2) = \frac{2\Big(\cos\left(\xi_2 y_1^\alpha\right) - \cos\left(\xi_2 y_2^\alpha\right) + \xi_2\left(y_1^\alpha - y_2^\alpha\right)\sin\left(\xi_2 y_1^\alpha\right)\Big)}{\xi_2^2(y_1^\alpha - y_2^\alpha)^2} \tag{54}$$

and

$$Q_2^\alpha(\xi_1,\xi_2) = \frac{2\Big(\sin\left(\xi_2 y_1^\alpha\right) - \sin\left(\xi_2 y_2^\alpha\right) - \xi_2\left(y_1^\alpha - y_2^\alpha\right)\cos\left(\xi_2 y_1^\alpha\right)\Big)}{\xi_2^2(y_1^\alpha - y_2^\alpha)^2}. \tag{55}$$

Case 2: $y_3^\alpha = y_2^\alpha$ and $\xi_1 = 0$

$$Q_1^\alpha(\xi_1,\xi_2) = \frac{2\Big(\cos\left(\xi_2 y_2^\alpha\right) - \cos\left(\xi_2 y_1^\alpha\right) - \xi_2\left(y_1^\alpha - y_2^\alpha\right)\sin\left(\xi_2 y_2^\alpha\right)\Big)}{\xi_2^2(y_1^\alpha - y_2^\alpha)^2} \tag{56}$$

and

$$Q_2^\alpha(\xi_1,\xi_2) = \frac{2\Big(\sin\left(\xi_2 y_2^\alpha\right) - \sin\left(\xi_2 y_1^\alpha\right) + \xi_2\left(y_1^\alpha - y_2^\alpha\right)\cos\left(\xi_2 y_2^\alpha\right)\Big)}{\xi_2^2(y_1^\alpha - y_2^\alpha)^2}. \tag{57}$$

Case 3: $y_2^\alpha = y_1^\alpha$ and $\xi_1 = 0$

$$Q_1^\alpha(\xi_1,\xi_2) = \frac{2\Big(\cos\left(\xi_2 y_1^\alpha\right) - \cos\left(\xi_2 y_3^\alpha\right) + \xi_2\left(y_1^\alpha - y_3^\alpha\right)\sin\left(\xi_2 y_1^\alpha\right)\Big)}{\xi_2^2(y_1^\alpha - y_3^\alpha)^2} \tag{58}$$

and

$$Q_2^\alpha(\xi_1,\xi_2) = \frac{2\Big(\sin\left(\xi_2 y_1^\alpha\right) - \sin\left(\xi_2 y_3^\alpha\right) - \xi_2\left(y_1^\alpha - y_3^\alpha\right)\cos\left(\xi_2 y_1^\alpha\right)\Big)}{\xi_2^2(y_1^\alpha - y_3^\alpha)^2}. \tag{59}$$

Case 4: $x_3^\alpha = x_1^\alpha$ and $\xi_2 = 0$

$$Q_1^\alpha(\xi_1,\xi_2) = \frac{2\Big(\cos\left(\xi_1 x_1^\alpha\right) - \cos\left(\xi_1 x_2^\alpha\right) + \xi_1\left(x_1^\alpha - x_2^\alpha\right)\sin\left(\xi_1 x_1^\alpha\right)\Big)}{\xi_1^2(x_1^\alpha - x_2^\alpha)^2} \tag{60}$$

and

$$Q_2^\alpha(\xi_1,\xi_2) = \frac{2\Big(\sin\left(\xi_1 x_1^\alpha\right) - \sin\left(\xi_1 x_2^\alpha\right) - \xi_1\left(x_1^\alpha - x_2^\alpha\right)\cos\left(\xi_1 x_1^\alpha\right)\Big)}{\xi_1^2(x_1^\alpha - x_2^\alpha)^2}. \tag{61}$$

Case 5: $x_3^\alpha = x_2^\alpha$ and $\xi_2 = 0$

$$Q_1^\alpha(\xi_1,\xi_2) = \frac{2\Big(\cos\left(\xi_1 x_2^\alpha\right) - \cos\left(\xi_1 x_1^\alpha\right) - \xi_1\left(x_1^\alpha - x_2^\alpha\right)\sin\left(\xi_1 x_2^\alpha\right)\Big)}{\xi_1^2(x_1^\alpha - x_2^\alpha)^2} \tag{62}$$

and

$$Q_2^{\alpha}(\xi_1,\xi_2) = \frac{2\Big(\sin\left(\xi_1 x_2^{\alpha}\right) - \sin\left(\xi_1 x_1^{\alpha}\right) + \xi_1\left(x_1^{\alpha} - x_2^{\alpha}\right)\cos\left(\xi_1 x_2^{\alpha}\right)\Big)}{\xi_1^2 (x_1^{\alpha} - x_2^{\alpha})^2}. \tag{63}$$

Case 6: $x_2^\alpha = x_1^\alpha$ and $\xi_2 = 0$

$$Q_1^\alpha(\xi_1,\xi_2) = \frac{2\Big(\cos\left(\xi_1 x_1^\alpha\right) - \cos\left(\xi_1 x_3^\alpha\right) + \xi_1\left(x_1^\alpha - x_3^\alpha\right)\sin\left(\xi_1 x_1^\alpha\right)\Big)}{\xi_1^2(x_1^\alpha - x_3^\alpha)^2} \tag{64}$$

and

$$Q_2^\alpha(\xi_1,\xi_2) = \frac{2\Big(\sin\left(\xi_1 x_1^\alpha\right) - \sin\left(\xi_1 x_3^\alpha\right) - \xi_1\left(x_1^\alpha - x_3^\alpha\right)\cos\left(\xi_1 x_1^\alpha\right)\Big)}{\xi_1^2(x_1^\alpha - x_3^\alpha)^2}. \tag{65}$$

Case 7: $\xi_1\left(x_1^\alpha - x_2^\alpha\right) + \xi_2\left(y_1^\alpha - y_2^\alpha\right) = 0$

$$\begin{aligned} Q_1^\alpha(\xi_1,\xi_2) \;=\; 2\Bigg(& \frac{(x_1^\alpha - x_2^\alpha)^2\cos\left(\dfrac{\xi_2(x_1^\alpha y_2^\alpha - x_2^\alpha y_1^\alpha)}{(x_1^\alpha - x_2^\alpha)}\right)}{\xi_2^2\Big(x_1^\alpha\left(y_2^\alpha - y_3^\alpha\right) - x_2^\alpha\left(y_1^\alpha - y_3^\alpha\right) - x_3^\alpha\left(y_2^\alpha - y_1^\alpha\right)\Big)^2} - \\ & - \frac{(x_1^\alpha - x_2^\alpha)^2\cos\left(\dfrac{\xi_2\Big(x_3^\alpha\left(y_1^\alpha - y_2^\alpha\right) - y_3^\alpha\left(x_1^\alpha - x_2^\alpha\right)\Big)}{(x_1^\alpha - x_2^\alpha)}\right)}{\xi_2^2\Big(x_1^\alpha\left(y_2^\alpha - y_3^\alpha\right) - x_2^\alpha\left(y_1^\alpha - y_3^\alpha\right) - x_3^\alpha\left(y_2^\alpha - y_1^\alpha\right)\Big)^2} + \\ & + \frac{(x_1^\alpha - x_2^\alpha)\sin\left(\dfrac{\xi_2(x_1^\alpha y_2^\alpha - x_2^\alpha y_1^\alpha)}{(x_1^\alpha - x_2^\alpha)}\right)}{\xi_2\Big(x_1^\alpha\left(y_2^\alpha - y_3^\alpha\right) - x_2^\alpha\left(y_1^\alpha - y_3^\alpha\right) - x_3^\alpha\left(y_2^\alpha - y_1^\alpha\right)\Big)}\Bigg) \end{aligned} \tag{66}$$

and

$$\begin{aligned} Q_2^\alpha(\xi_1,\xi_2) \;=\; 2\Bigg(& \frac{(x_1^\alpha - x_2^\alpha)^2\sin\left(\dfrac{\xi_2(x_1^\alpha y_2^\alpha - x_2^\alpha y_1^\alpha)}{(x_1^\alpha - x_2^\alpha)}\right)}{\xi_2^2\Big(x_1^\alpha\left(y_2^\alpha - y_3^\alpha\right) - x_2^\alpha\left(y_1^\alpha - y_3^\alpha\right) - x_3^\alpha\left(y_2^\alpha - y_1^\alpha\right)\Big)^2} + \\ & + \frac{(x_1^\alpha - x_2^\alpha)^2\sin\left(\dfrac{\xi_2\Big(x_3^\alpha\left(y_1^\alpha - y_2^\alpha\right) - y_3^\alpha\left(x_1^\alpha - x_2^\alpha\right)\Big)}{(x_1^\alpha - x_2^\alpha)}\right)}{\xi_2^2\Big(x_1^\alpha\left(y_2^\alpha - y_3^\alpha\right) - x_2^\alpha\left(y_1^\alpha - y_3^\alpha\right) - x_3^\alpha\left(y_2^\alpha - y_1^\alpha\right)\Big)^2} - \\ & - \frac{(x_1^\alpha - x_2^\alpha)\cos\left(\dfrac{\xi_2(x_1^\alpha y_2^\alpha - x_2^\alpha y_1^\alpha)}{(x_1^\alpha - x_2^\alpha)}\right)}{\xi_2\Big(x_1^\alpha\left(y_2^\alpha - y_3^\alpha\right) - x_2^\alpha\left(y_1^\alpha - y_3^\alpha\right) - x_3^\alpha\left(y_2^\alpha - y_1^\alpha\right)\Big)}\Bigg). \end{aligned} \tag{67}$$

Case 8: $\xi_1\left(x_2^\alpha - x_3^\alpha\right) + \xi_2\left(y_2^\alpha - y_3^\alpha\right) = 0$

$$
\begin{aligned}
Q_1^\alpha(\xi_1,\xi_2) \;=\; 2\Bigg(& \frac{(x_2^\alpha - x_3^\alpha)^2 \cos\left(\dfrac{\xi_2(x_2^\alpha y_3^\alpha - x_3^\alpha y_2^\alpha)}{(x_2^\alpha - x_3^\alpha)}\right)}{\xi_2^2\Big(x_1^\alpha\,(y_2^\alpha - y_3^\alpha) - x_2^\alpha\,(y_1^\alpha - y_3^\alpha) - x_3^\alpha\,(y_2^\alpha - y_1^\alpha)\Big)^2} - \\
& \frac{(x_2^\alpha - x_3^\alpha)^2 \cos\left(\dfrac{\xi_2\Big(x_1^\alpha\,(y_2^\alpha - y_3^\alpha) - y_1^\alpha\,(x_2^\alpha - x_3^\alpha)\Big)}{(x_2^\alpha - x_3^\alpha)}\right)}{\xi_2^2\Big(x_1^\alpha\,(y_2^\alpha - y_3^\alpha) - x_2^\alpha\,(y_1^\alpha - y_3^\alpha) - x_3^\alpha\,(y_2^\alpha - y_1^\alpha)\Big)^2} + \\
& + \frac{(x_1^\alpha - x_2^\alpha) \sin\left(\dfrac{\xi_2(x_2^\alpha y_3^\alpha - x_3^\alpha y_2^\alpha)}{(x_2^\alpha - x_3^\alpha)}\right)}{\xi_2\Big(x_1^\alpha\,(y_2^\alpha - y_3^\alpha) - x_2^\alpha\,(y_1^\alpha - y_3^\alpha) - x_3^\alpha\,(y_2^\alpha - y_1^\alpha)\Big)}\Bigg)
\end{aligned}
\tag{68}
$$

and

$$
\begin{aligned}
Q_2^\alpha(\xi_1,\xi_2) \;=\; 2\Bigg(& \frac{(x_2^\alpha - x_3^\alpha)^2 \sin\left(\dfrac{\xi_2(x_2^\alpha y_3^\alpha - x_3^\alpha y_2^\alpha)}{(x_2^\alpha - x_3^\alpha)}\right)}{\xi_2^2\Big(x_1^\alpha\,(y_2^\alpha - y_3^\alpha) - x_2^\alpha\,(y_1^\alpha - y_3^\alpha) - x_3^\alpha\,(y_2^\alpha - y_1^\alpha)\Big)^2} + \\
& + \frac{(x_2^\alpha - x_3^\alpha)^2 \sin\left(\dfrac{\xi_2\Big(x_1^\alpha\,(y_2^\alpha - y_3^\alpha) - y_1^\alpha\,(x_2^\alpha - x_3^\alpha)\Big)}{(x_2^\alpha - x_3^\alpha)}\right)}{\xi_2^2\Big(x_1^\alpha\,(y_2^\alpha - y_3^\alpha) - x_2^\alpha\,(y_1^\alpha - y_3^\alpha) - x_3^\alpha\,(y_2^\alpha - y_1^\alpha)\Big)^2} - \\
& - \frac{(x_2^\alpha - x_3^\alpha) \cos\left(\dfrac{\xi_2(x_2^\alpha y_3^\alpha - x_3^\alpha y_2^\alpha)}{(x_2^\alpha - x_3^\alpha)}\right)}{\xi_2\Big(x_1^\alpha\,(y_2^\alpha - y_3^\alpha) - x_2^\alpha\,(y_1^\alpha - y_3^\alpha) - x_3^\alpha\,(y_2^\alpha - y_1^\alpha)\Big)}\Bigg).
\end{aligned}
\tag{69}
$$

Case 9: $\xi_1\,(x_1^\alpha - x_3^\alpha) + \xi_2\,(y_1^\alpha - y_3^\alpha) = 0$

$$
\begin{aligned}
Q_1^\alpha(\xi_1,\xi_2) \;=\; 2\Bigg(& \frac{(x_1^\alpha - x_3^\alpha)^2 \cos\left(\dfrac{\xi_2(x_1^\alpha y_3^\alpha - x_3^\alpha y_1^\alpha)}{(x_1^\alpha - x_3^\alpha)}\right)}{\xi_2^2\Big(x_1^\alpha\,(y_2^\alpha - y_3^\alpha) - x_2^\alpha\,(y_1^\alpha - y_3^\alpha) - x_3^\alpha\,(y_2^\alpha - y_1^\alpha)\Big)^2} - \\
& \frac{(x_1^\alpha - x_3^\alpha)^2 \cos\left(\dfrac{\xi_2\Big(x_2^\alpha\,(y_3^\alpha - y_1^\alpha) - y_2^\alpha\,(x_3^\alpha - x_1^\alpha)\Big)}{(x_1^\alpha - x_3^\alpha)}\right)}{\xi_2^2\Big(x_1^\alpha\,(y_2^\alpha - y_3^\alpha) - x_2^\alpha\,(y_1^\alpha - y_3^\alpha) - x_3^\alpha\,(y_2^\alpha - y_1^\alpha)\Big)^2} +
\end{aligned}
$$

$$+\frac{(x_1^\alpha - x_3^\alpha)\sin\left(\frac{\xi_2(x_1^\alpha y_3^\alpha - x_3^\alpha y_1^\alpha)}{(x_1^\alpha - x_3^\alpha)}\right)}{\xi_2\Big(x_1^\alpha\,(y_2^\alpha - y_3^\alpha) - x_2^\alpha\,(y_1^\alpha - y_3^\alpha) - x_3^\alpha\,(y_2^\alpha - y_1^\alpha)\Big)}\Bigg) \tag{70}$$

and

$$\begin{aligned} Q_2^\alpha(\xi_1,\xi_2) \;=\; 2\Bigg(& -\frac{(x_1^\alpha - x_3^\alpha)^2\sin\left(\frac{\xi_2(x_1^\alpha y_3^\alpha - x_3^\alpha y_1^\alpha)}{(x_1^\alpha - x_3^\alpha)}\right)}{\xi_2^2\Big(x_1^\alpha\,(y_2^\alpha - y_3^\alpha) - x_2^\alpha\,(y_1^\alpha - y_3^\alpha) - x_3^\alpha\,(y_2^\alpha - y_1^\alpha)\Big)^2} + \\ & +\frac{(x_1^\alpha - x_3^\alpha)^2\sin\left(\frac{\xi_2\Big(x_2^\alpha\,(y_3^\alpha - y_1^\alpha) - y_2^\alpha\,(x_3^\alpha - x_1^\alpha)\Big)}{(x_1^\alpha - x_3^\alpha)}\right)}{\xi_2^2\Big(x_1^\alpha\,(y_2^\alpha - y_3^\alpha) - x_2^\alpha\,(y_1^\alpha - y_3^\alpha) - x_3^\alpha\,(y_2^\alpha - y_1^\alpha)\Big)^2} + \\ & +\frac{(x_1^\alpha - x_3^\alpha)\cos\left(\frac{\xi_2(x_1^\alpha y_3^\alpha - x_3^\alpha y_1^\alpha)}{(x_1^\alpha - x_3^\alpha)}\right)}{\xi_2\Big(x_1^\alpha\,(y_2^\alpha - y_3^\alpha) - x_2^\alpha\,(y_1^\alpha - y_3^\alpha) - x_3^\alpha\,(y_2^\alpha - y_1^\alpha)\Big)}\Bigg). \end{aligned} \tag{71}$$

	825	819	835	838	835	819	825
	937	877	741	689	741	877	937
	1132	1192	1339	1394	1339	1192	1132
σ^0_{11} ⇐	1210	1216	1171	1157	1171	1216	1210
	1132	1192	1339	1394	1339	1192	1132
	937	877	741	689	741	877	937
	825	819	835	838	835	819	825

σ^0_{11} = 100 MPa ⇒

(a) Unit cell of 49 squares subvolumes with 9 squaresubvolumes in the center embedded in 40 square subvolumes.

	819 / 832	815 / 821	836 / 831	846 / 826	841 / 826	818 / 819	816 / 836
	913 / 965	868 / 891	797 / 676	723 / 630	753 / 723	833 / 934	905 / 973
	1100 / 1161	1152 / 1224	1367 / 1318	1430 / 1376	1429 / 1265	1175 / 1193	1108 / 1152
σ^0_{11} ⇐	1204 / 1209	1218 / 1203	1202 / 1158	1166 / 1166	1158 / 1202	1203 / 1218	1209 / 1204
	1152 / 1108	1193 / 1175	1265 / 1429	1376 / 1430	1318 / 1367	1224 / 1152	1161 / 1100
	973 / 905	934 / 833	723 / 753	630 / 723	676 / 797	891 / 868	965 / 913
	836 / 816	819 / 818	826 / 841	826 / 846	831 / 836	821 / 815	832 / 819

σ^0_{11} = 1000 kPa ⇒

(b) Unit cell of 98 trianglar subvolumes with 18 triangular subvolumes in the center embedded in 80 square subvolumes.

Figure 1.—Transverse stress concentration, σ_{11}, for an applied stress of σ^0_{11} = 1000 kPa at an overall stressed rate of σ^0_{11} = 1000 MPa per second. Each unit cell is embedded in a doubly-periodic array of identical cells. The subvolumes in the center of the unit cell represent a tungsten fiber of square planform embedded in subvolumes representing a copper matrix.

83	82	84	84	84	82	83
94	88	74	69	74	88	94
113	119	134	139	134	119	113
121	122	117	116	117	122	121
113	119	134	139	134	119	113
94	88	74	69	74	88	94
82	82	84	84	84	82	83

$\Leftarrow \sigma_{11}^0$ $\quad \sigma_{11}^0 =$ 100 MPa $\Rightarrow$

(a) Transverse stress concentration.

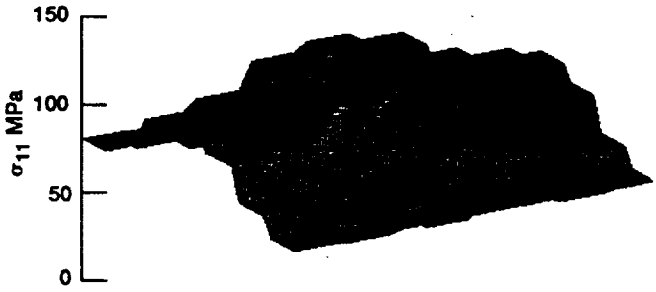

(b) Topological plot.

Figure 2.—Transverse stress concentration, σ_{11}, for an applied stress of $\sigma_{11}^0 = 100$ MPa at an overall loading rate of $\dot{\sigma}_{11}^0 =$ 10 MPa per second, and topological plot of the numerical stresses.

35	31	25	22	25	31	35
40	35	19	16	19	35	40
46	52	25	32	25	52	46
49	54	16	23	16	54	49
46	52	25	32	25	52	46
40	35	19	16	19	35	40
35	31	25	22	25	31	35

$\Leftarrow \sigma_{11}^0$ $\quad \sigma_{11}^0 =$ 100 MPa $\Rightarrow$

(a) Hydrostatic stress concentration.

(b) Topological plot.

Figure 3.—Hydrostatic stress concentration, $(\sigma_{11} + \sigma_{22} + \sigma_{33})/3$, for an applied stress of $\sigma_{11}^0 = 100$ MPa per second applied at an overall loading rate of $\dot{\sigma}_{11}^0 = 10$ MPa per second, and topological plot of the numerical stresses.

76	70	68	61	68	70	76
103	89	52	43	52	89	103
111	126	181	202	181	126	111
119	130	98	88	98	130	119
111	126	181	202	181	126	111
103	89	52	43	52	89	103
76	70	68	61	68	70	76

$\sigma_{11}^0 \Leftarrow$ $\sigma_{11}^0 = 100$ MPa $\Rightarrow$

(a) Transverse stress concentration.

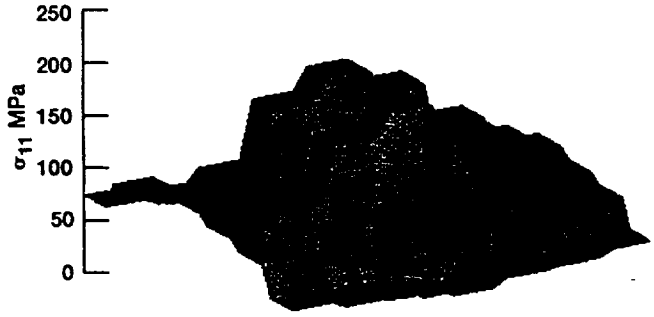

(b) Topological plot.

Figure 4.—Transverse stress concentration, σ_{11}, for an applied stress of σ_{11}^0 =100 MPa at an overall loading rate of $\dot{\sigma}_{11}^0$= 10 MPa per second after 3600 seconds of creep at 100 MPa, and topological plot of the numerical stresses.

41	27	22	13	22	27	41
60	46	8	0	8	46	60
64	80	-9	31	-9	80	64
70	85	-52	-13	-52	85	70
64	80	-9	31	-9	80	64
60	46	8	0	8	46	60
41	27	22	13	22	27	41

$\sigma_{11}^0 \Leftarrow$ $\sigma_{11}^0 = 100$ MPa $\Rightarrow$

(a) Hydrostratic stress concentration.

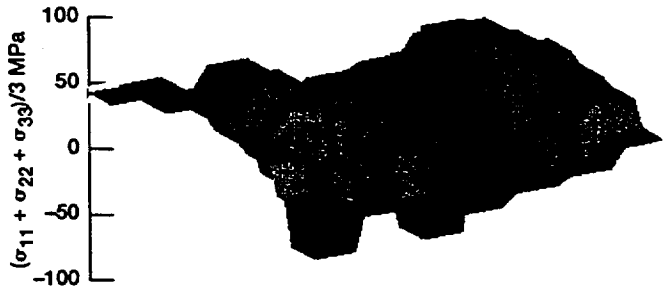

(b) Topological plot.

Figure 5.—Hydrostatic stress concentration, $\sigma_{11} + \sigma_{22} + \sigma_{33})/3$, for an applied stress of σ_{11}^0 = 100 MPa per second applied at an overall loading rate of $\dot{\sigma}_{11}^0$ = 10 MPa per second, after 3600 seconds of creep at 100 MPa and topological plot of the numerical stresses.

-6	-12	-16	-23	-16	-12	-6
9	1	-22	-26	-22	1	9
-2	7	47	63	47	7	-2
-2	8	-19	-28	-19	8	-2
-2	7	47	63	47	7	-2
9	1	-22	-26	-22	1	9
-6	-12	-16	-23	-16	-12	-6

$\Leftarrow \sigma^0_{11}$ $\quad \sigma^0_{11} =$ 100 MPa $\Rightarrow$

(a) Transverse stress concentration.

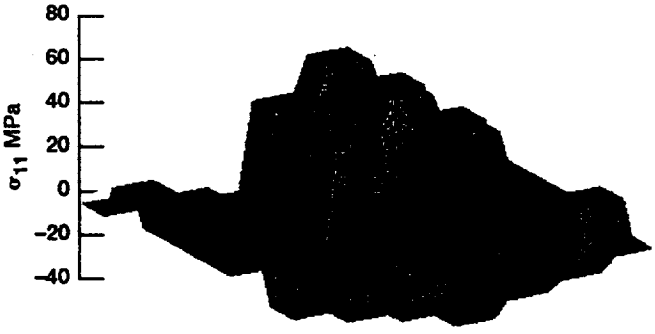

(b) Topological plot.

Figure 6.—Transverse stress concentration after unloading to a zero overall stress rate of $\dot{\sigma}^0_{11} = -10$ MPa from the state depicted in Fig 4, and topological plot of the numerical stresses.

6	-4	-3	-9	-3	-4	6
21	10	-11	-16	-11	10	21
18	28	-34	-1	-34	28	18
21	31	-69	-36	-69	31	21
18	28	-34	-1	-34	28	18
21	10	-11	-16	-11	10	21
6	-4	-3	-9	-3	-4	6

$\Leftarrow \sigma^0_{11}$ $\quad \sigma^0_{11} =$ 100 MPa $\Rightarrow$

(a) Hydrostatic stress concentration.

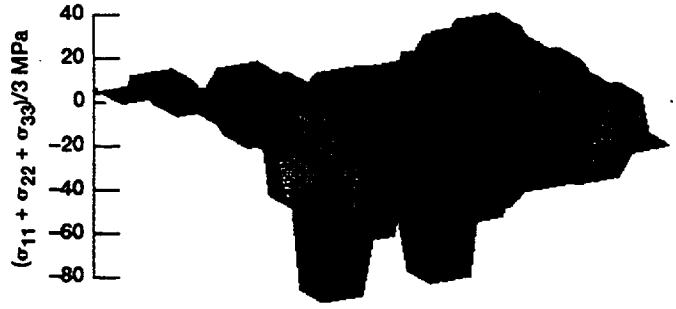

(b) Topological plot.

Figure 7.—Hydrostatic stress concentration after unloading to a zero overall stress at an overall stress rate of $\dot{\sigma}^0_{11} =$ −10 MPa from the state depicted in Fig. 5, and topological plot of the numeric stresses.

REPORT DOCUMENTATION PAGE

Form Approved
OMB No. 0704-0188

1. AGENCY USE ONLY (*Leave blank*)	2. REPORT DATE	3. REPORT TYPE AND DATES COVERED
	March 1993	Technical Memorandum

4. TITLE AND SUBTITLE

Thermoviscoplastic Analysis of Fibrous Periodic Composites Using Triangular Subvolumes

5. FUNDING NUMBERS

WU-505-63-5A

6. AUTHOR(S)

Kevin P. Walker, Alan D. Freed, and Eric H. Jordan

7. PERFORMING ORGANIZATION NAME(S) AND ADDRESS(ES)

National Aeronautics and Space Administration
Lewis Research Center
Cleveland, Ohio 44135-3191

8. PERFORMING ORGANIZATION REPORT NUMBER

E-7686

9. SPONSORING/MONITORING AGENCY NAMES(S) AND ADDRESS(ES)

National Aeronautics and Space Administration
Washington, D.C. 20546-0001

10. SPONSORING/MONITORING AGENCY REPORT NUMBER

NASA TM-106076

11. SUPPLEMENTARY NOTES

Kevin P. Walker, Engineering Science Software, Inc., Smithfield, Rhode Island 02917; Alan D. Freed, NASA Lewis Research Center; Eric H. Jordan, University of Connecticut, Storrs, Connecticut 06269. Responsible person, Alan D. Freed, (216) 433-8747.

12a. DISTRIBUTION/AVAILABILITY STATEMENT

Unclassified - Unlimited
Subject Category 24

12b. DISTRIBUTION CODE

13. ABSTRACT (*Maximum 200 words*)

The nonlinear viscoplastic behavior of fibrous periodic composites is analyzed by discretizing the unit cell into triangular subvolumes. A set of these subvolumes can be configured by the analyst to construct a representation for the unit cell of a periodic composite. In each step of the loading history the total strain increment at any point is governed by an integral equation which applies to the entire composite. A Fourier series approximation allows the incremental stresses and strains to be determined within a unit cell of the periodic lattice. The nonlinearity arising from the viscoplastic behavior of the constituent materials comprising the composite is treated as fictitious body force in the governing integral equation. Specific numerical examples showing the stress distributions in the unit cell of a fibrous tungsten/copper metal matrix composite under viscoplastic loading conditions are given. The stress distribution resulting in the unit cell when the composite material is subjected to an overall transverse stress loading history perpendicular to the fibers is found to be highly heterogeneous, and typical homogenization techniques based on treating the stress and strain distributions within the constituent phases as homogeneous result in large errors under inelastic loading conditions.

14. SUBJECT TERMS

Metal matrix composites; Creep analysis; Fourier analysis

15. NUMBER OF PAGES

28

16. PRICE CODE

A02

17. SECURITY CLASSIFICATION OF REPORT	18. SECURITY CLASSIFICATION OF THIS PAGE	19. SECURITY CLASSIFICATION OF ABSTRACT	20. LIMITATION OF ABSTRACT
Unclassified	Unclassified	Unclassified	